Applied Catalysis B: Environmental 146 (2014) 162–168

Contents lists available at ScienceDirect

Applied Catalysis B: Environmental

journal homepage: www.elsevier.com/locate/apcatb

A comparative study of reduced graphene oxide modified TiO_2, ZnO and Ta_2O_5 in visible light photocatalytic/photochemical oxidation of methylene blue

Hongqi Sun*, Shizhen Liu, Shaomin Liu, Shaobin Wang**

Department of Chemical Engineering, Curtin University, GPO Box U1987, Perth, WA 6845, Australia

ARTICLE INFO

Article history:
Received 26 October 2012
Received in revised form 11 February 2013
Accepted 14 March 2013
Available online 22 March 2013

Keywords:
Reduced graphene oxide
TiO_2
Photocatalysis
Photochemical
Methylene blue

ABSTRACT

Reduced graphene oxide (rGO) was applied to prepare various composites of rGO/photocatalyst of G/TiO_2, G/ZnO and G/Ta_2O_5, using titanium (IV) isopropoxide, Zn powder and commercial Ta_2O_5 powder as photocatalyst precursors, respectively. X-ray diffraction (XRD), field emission scanning electron microscopy (FE-SEM), Fourier transform infrared spectroscopy (FTIR), thermogravimetric-differential thermal analysis (TG-DTA) and UV–vis diffuse reflectance (UV–vis DRS) were employed to investigate the crystal structure, morphology, surface groups, rGO loading, and optical properties of the produced composites. The photocatalytic activities of the composites under UV–vis and visible light were studied in degradation of methylene blue (MB). G/Ta_2O_5 showed an enhanced efficiency under UV–vis irradiation. G/TiO_2 demonstrated an effective degradation of MB under visible light. The effects of various oxidants, peroxymonosulfate (PMS), peroxydisulfate (PDS) and hydrogen peroxide (H_2O_2) on MB degradation were thoroughly investigated. H_2O_2 was a promising oxidant for promoting MB degradation under visible light. The mechanism of the enhanced efficiency in the system of G/TiO_2 + vis + H_2O_2 was discussed.

1. Introduction

Light-assisted degradation of organic pollutants has been widely employed as a promising strategy for environmental remediation. Currently, direct ultraviolet (UV) light or sunlight photodegradation of organic pollutants has a very low efficiency, and highly depends on the photoreactivity of the specific substance [1]. The free radicals, such as hydroxyl [2], super oxygen [3], and sulfate radicals [4] produced from oxidants, however, are able to attack organic compounds almost non-selectively, with a high rate. Such advanced oxidation processes (AOPs) have been applied in photo-Fenton (UV/H_2O_2) [5], photocatalysis [6,7], and photochemical reactions [8–10]. Most photochemical oxidations involve homogeneous metal ions, such as Fe(II), Fe(III), Co(II) or Ag(I), etc. [5,11,12], however, the discharge of such metal ions into water bodies would lead to serious secondary contamination. It was found that heavy metal leaching could also occur in heterogeneous catalytic reactions [13–15].

The efficiency of light-assisted AOPs would be directly controlled by the production of free radicals, which significantly depend on the activation of photocatalysts and oxidants upon light irradiation. Conventional TiO_2 photocatalysis has barriers in practical remediation of organic pollutants due to the low efficiency in sunlight absorption [16]. Increasing the photoinduced carriers' separation rate and extending the absorption threshold of TiO_2 were proposed to overcome the barriers in TiO_2 photocatalysis. To this end, a variety of methods, e.g., metal doping, noble metal deposition, semiconductor coupling, dye sensitizing, and non-metal modification, have been attempted [6,7,16]. In general, visible light photocatalysis on TiO_2 can be facilitated by introducing additional electronic states and higher activity can be realized by creating electronic interactions between TiO_2 and modifying materials, such as dye, noble metal, narrow band semiconductor, etc. [17].

ZnO and Ta_2O_5 are also popular photocatalysts, which can only work in UV region [18,19]. The strategies for making ZnO responsive to visible light are very similar to those of TiO_2, including doping [20], dye sensitizing[21], and semiconductor coupling [22], etc. On the other hand, the modification of Ta_2O_5 for visible light photocatalysis has been less successful, and only a few investigations have been reported [23–25].

As a new carbonaceous material, graphene has attracted tremendous attention in the past years, due to its unique electronic property, excellent mobility of charge carriers (200,000 $cm^2 V^{-1} s^{-1}$), and extremely high theoretical specific surface area (~2600 $m^2 g^{-1}$) [26]. It was reported that these salient features can be employed to improve electronic, optoelectronic,

* Corresponding author.
** Corresponding author. Tel.: +61 8 9266 3776; fax: +61 8 9266 2681.
E-mail addresses: h.sun@curtin.edu.au (H. Sun), shaobin.wang@curtin.edu.au (S. Wang).

0926-3373/$ – see front matter © 2013 Elsevier B.V. All rights reserved.
http://dx.doi.org/10.1016/j.apcatb.2013.03.027

electrocatalytic, and photocatalytic performance of semiconductor materials [27]. Zhang et al. [28] reported a facile one-step hydrothermal method for preparation of a chemically bonded TiO_2(P25)–graphene nanocomposite, which had great adsorptivity of dyes, extended light absorption, and efficient charge separation. Stengl et al. [29] prepared a nonstoichiometric TiO_2–graphene nanocomposite by thermal hydrolysis of suspension with graphene nanosheets and titania–peroxo complex. The direct interaction between TiO_2 and graphene prevented the reaggregation of the graphene sheets, resulting in a higher photocatalytic activity. Lee et al. [30] reported that graphene-wrapped anatase TiO_2 nanoparticles presented a high photocatalytic activity under visible light irradiation. Zhao et al. [31] suggested that a "dyade"-like structure would form on graphene@TiO_2 to produce more OH radicals than pure TiO_2 under UV and visible-light irradiation. Some investigations in graphene/ZnO were also attempted [32–34]. However, no investigation in graphene/Ta_2O_5 has been reported.

On the other hand, graphene itself can significantly contribute to chemical oxidation of organic pollutants. In a pioneering study, we discovered that chemically reduced graphene oxide was able to effectively activate peroxymonosulfate (PMS) to produce active sulfate radicals. Graphene demonstrated a higher activity than several other carbon allotropes, such as activated carbon, graphite powder, graphene oxide, and multiwall carbon nanotube, as well as a cobalt oxide, in oxidation of phenol solutions [35]. In addition, previous studies demonstrated that effective remediation of organic pollutants can be conducted over photocatalyst/oxidant [8], supported photocatalyst/oxidant [9], and photocatalyst supported cobalt/oxidant [10].

Therefore, it would be of great interest to investigate the effect of reduced graphene oxide (rGO) on the photocatalytic and photochemical performance of different photocatalysts. In this paper, we reported the preparation of several photocatalysts, graphene/TiO_2, graphene/ZnO, and graphene/Ta_2O_5 and compared their photocatalytic performances under UV and visible irradiations. Moreover, the photochemical activity of graphene/TiO_2 was further investigated in the presence of several oxidants, peroxymonosulfate (PMS), peroxydisulfate (PDS) and hydrogen peroxide (H_2O_2) under visible light irradiations.

2. Experimental

2.1. Sample preparation

Graphene oxide (GO) was prepared by a modified Hummers method [36,37] and the reduction of exfoliated GO was obtained by a hydrothermal reaction using hydrazine hydrate. Typically, GO (100 mg) was loaded in a 250 mL round bottom flask with 100 mL of deionized water and subjected to ultrasonic treatment for 2 h, yielding a homogeneous yellow-brown dispersion. Hydrazine hydrate (1.00 mL) was then added in and the solution was heated at 100 °C for 24 h. The reduced GO (rGO) was gradually precipitated as a black solid. This product was separated by filtration and washed with ethanol and water several times and then dried at 80 °C.

For synthesis of G/TiO_2, rGO powder, cetyl trimethylammonium bromide (CTAB, 0.5 g) and 30 mL of ethanol were placed in a 100 mL of beaker with stirring. After 30 min, titanium (IV) isopropoxide was dropwised into the reactor. Then 20 mL of deionized water was added into the mixed solution. The suspension was stirred for 8 h and dried at 80 °C. The solid was annealed in a muffle furnace at 500 °C for 5 min. The loading of graphene was kept at 3 wt%.

G(3 wt%)/Ta_2O_5 was synthesized by the similar method to G(3 wt%)/TiO_2 sample, except that commercial Ta_2O_5 powders were used as a precursor of photocatalyst.

For synthesis of G(3 wt%)/ZnO, 0.64 g of zinc powders and 0.04 g of GO were mixed in a beaker, then CTAB was added at a concentration of 0.1 M. The mixture was magnetically stirred for 2 h, and then transferred into a 120 mL of a Teflon-lined stainless steel autoclave. Hydrothermal reaction was carried out at 195 °C for 24 h. A gray-black precipitate was collected by filtration and washed with ethanol/water. The resulted G(3 wt%)/ZnO photocatalyst was dried at 60 °C in air.

2.2. Characterization

The crystalline structure of samples was analyzed by powder X-ray diffraction (XRD) using a Bruker D8-Advance X-ray diffractometer with Cu Kα radiation (λ = 1.5418 Å) operated at 40 kV and 30 mA, respectively. FTIR analysis was performed on a Perkin-Elmer Model FTIR-100 with a MIR detector. UV–vis diffuse reflectance spectra (DRS) of samples were recorded on a JASCO V670 spectrophotometer with an Ø 60 mm integrating sphere and $BaSO_4$ as a reference material. Field emission scanning electron microscopy (FE-SEM), performed on a Zeiss Neon 40EsB, was used to evaluate the morphology, size and texture information of the samples. Thermogravimetric-differential thermal analysis (TG-DTA) was carried out on a TGA/DSC 1 instrument of Mettler-Toledo in air flow at a heating rate of 10 °C/min.

2.3. Photocatalytic and photochemical tests

Photocatalytic performances of various catalysts were evaluated in the photodegradation of methylene blue (MB) under either artificial solar light or visible light. In a typical process, aqueous solution of MB (10 mg/L, 200 mL) and photocatalysts (100 mg) were put into a 1-L double-jacket cylindrical reactor with cycled cooling water (25 °C) and stirring. The photoreaction vessel was positioned 30 cm away from the radiation source with a cut-off filter. Two light sources were used, one is UV–vis light with intensities at 2.31 μW/cm^2 (220–280 nm), 6.94 mW/cm^2 (315–400 nm), and 129.3 mW/cm^2 (400–1050 nm) and the other is visible light with an intensity of 84 mW/cm^2 at 400–1050 nm. The reaction solution was firstly stirred for 30 min in dark to achieve adsorption equilibrium. The photocatalytic reaction was then started by turning on a halogen lamp. In a photochemical reaction, oxidants (PMS or PDS at 2 g/L, or H_2O_2 at varying amounts) were added into the reaction solution just before switching on the light. At given time intervals, reacting solution was centrifuged and analyzed for MB concentration on a JASCO UV–vis spectrophotometer at a wavelength of 664 nm.

3. Results and discussion

3.1. Characterization of graphene/photocatalyst composites

Fig. 1 shows XRD patterns of three rGO/photocatalyst composites. Fig. 1(A) shows that G(3 wt%)/TiO_2 was of anatase crystalline phase, owing to the calcination at 500 °C for 5 min. The crystal faces of [1 0 3], [1 1 2], [1 0 5] and [2 1 1] did not grow very well, due to the short-time calcination. Brookite [1 2 1] phase was found at 2θ of 30.7°, due to the short period of calcination of 5 min in the preparation of G(3 wt%)/TiO_2 [38]. It has been reported that the brookite phase will disappear once the duration is prolonged to several hours [39,40]. The average crystallite size of anatase TiO_2 was estimated by the Scherrer's equation: $D = K\lambda/\beta\cos\theta$ to be 9.3 nm. In general, the characteristic reflection of GO is close to 2θ of 10°, with other two weak peaks at about 26° and 43° [35,41]. In this study, neither diffraction of GO nor rGO was observed in XRD pattern, possibly due to the low content (<3 wt%) of rGO loading.

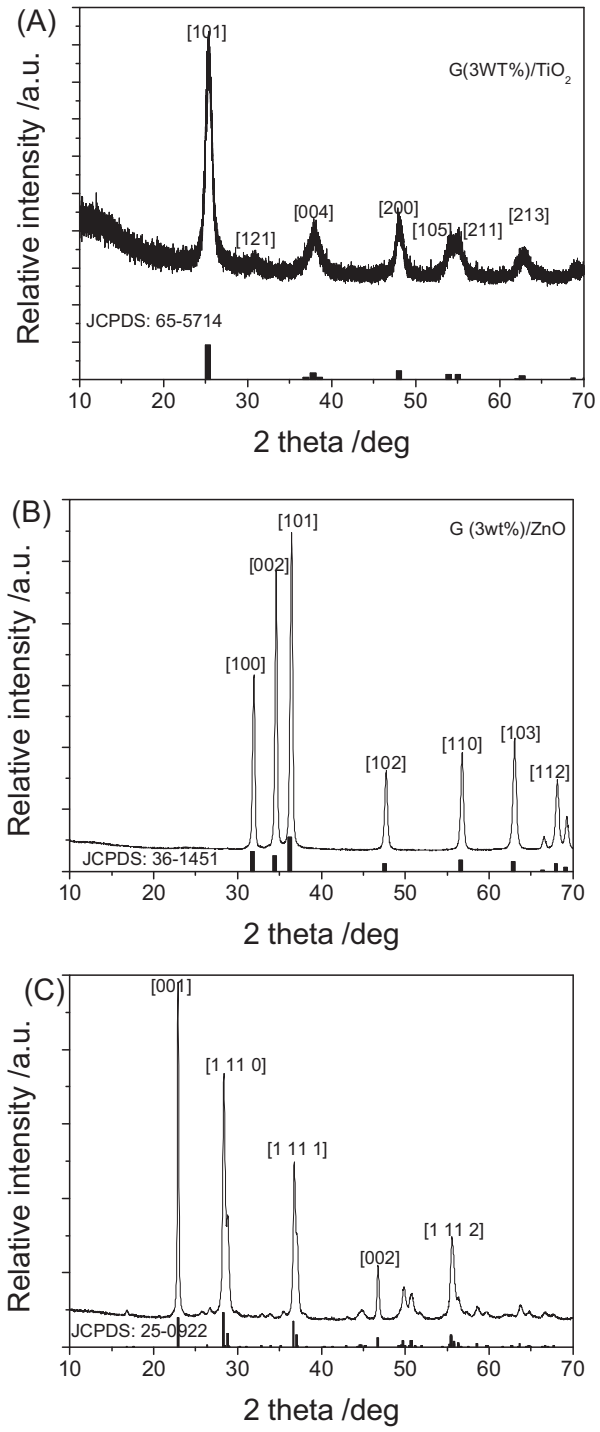

Fig. 1. XRD patterns of G/TiO_2 (A), G/ZnO (B), and G/Ta_2O_5 (C).

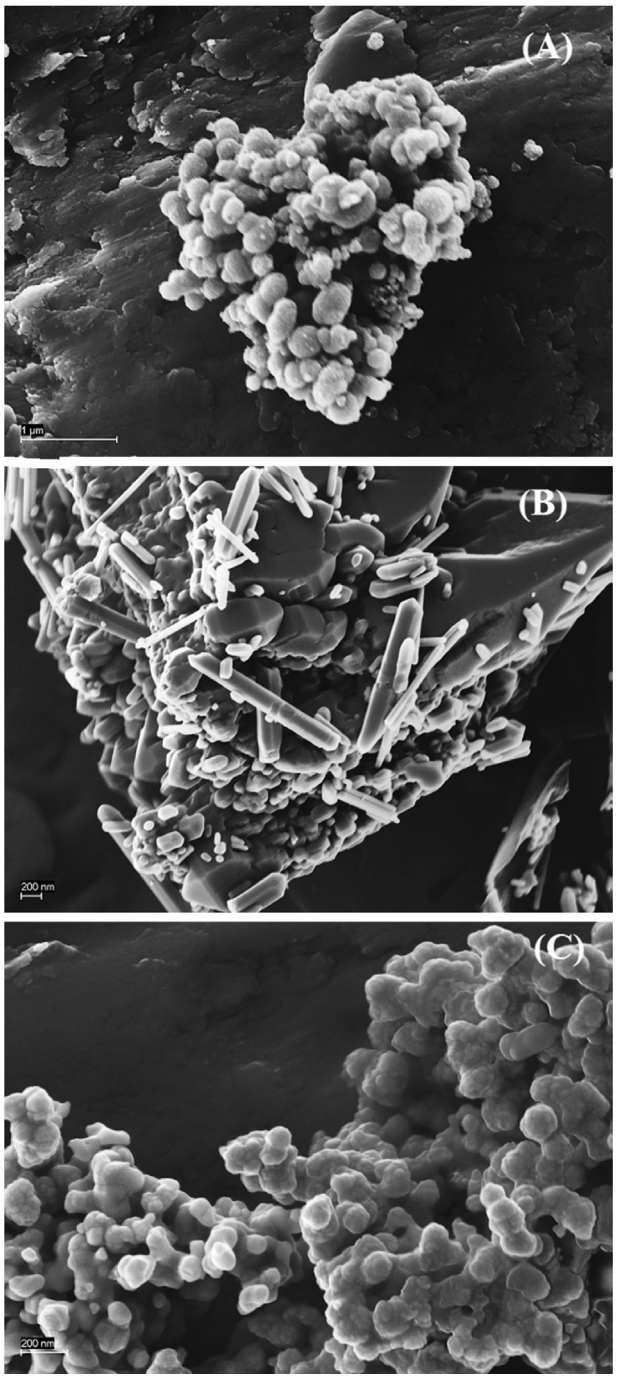

Fig. 2. SEM images of G/TiO_2 (A), G/ZnO (B), and G/Ta_2O_5 (C).

Fig. 1(B) indicates that ZnO crystallites were grown very well via the hydrothermal process. The peaks of $2\theta = 31.9^\circ$, 34.6°, 36.4°, 47.7°, 56.8°, 63.0° and 68.1° can be indexed to the crystal faces of [1 0 0], [0 0 2], [1 0 1], [1 0 2], [1 1 0], [1 0 3] and [1 1 2] of ZnO, respectively [9,42]. Similar to G/TiO_2, no GO or rGO peaks were observed. The crystallite size of ZnO was estimated by the Scherrer's equation to be 31.8 nm. Fig. 1(C) shows that graphene modification of Ta_2O_5 did not significantly change the crystal structure of the commercial Ta_2O_5 powders. Major peaks were found at $2\theta = 22.9^\circ$, 28.5°, 36.7°, 46.7°, 49.9°, 51.0°, and 55.8°, which are assigned to the faces of [0 0 1], [1 1 1 0], [1 1 1 1], [0 0 2], [0 2 2 0], [2 1 5 1] and [1 1 1 2] of orthorhombic Ta_2O_5, respectively [43]. The crystallite size of Ta_2O_5 was 63.9 nm.

Fig. 2 shows SEM images of three rGO/photocatalyst composites to illustrate their morphological information. TiO_2 and Ta_2O_5 presented as spherical particles with significant aggregation, while ZnO showed rod-like morphology at a length of 1–5 μm. The morphology of rGO in G/ZnO was better shaped than those in G/TiO_2 or G/Ta_2O_5, and the better framework of G/ZnO was also observed. Such a structure was formed due to hydrothermal process without calcination, while both G/TiO_2 and G/Ta_2O_5 went through a calcination, which might cause structural destruction in graphene.

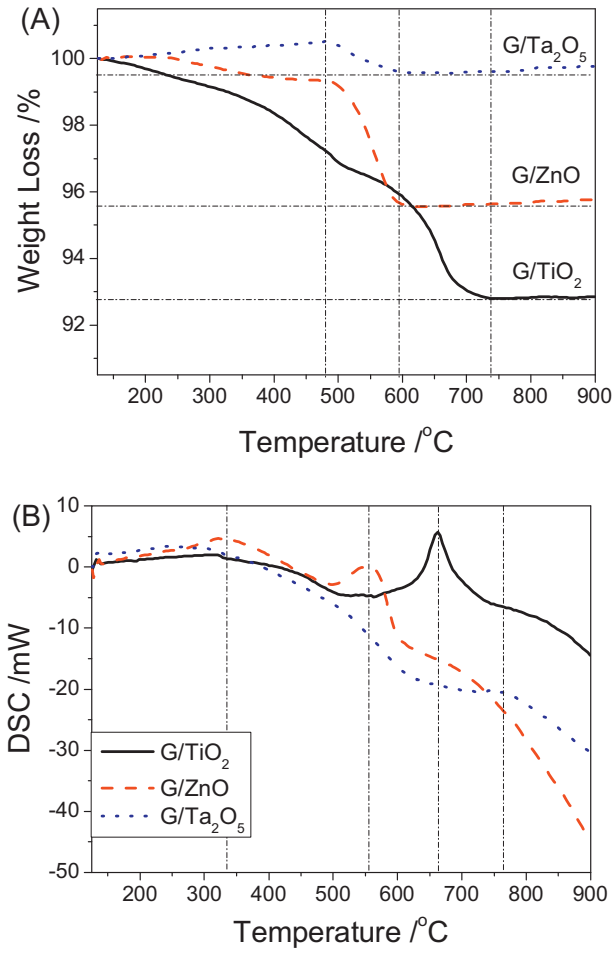

Fig. 3. TG/DSC diagram of the three composites of G/TiO_2, G/ZnO and G/Ta_2O_5. (A): TG, (B): DTA.

TG-DSC was conducted to evaluate the thermal properties of rGO in the composites. TGA curve of rGO (not shown here) shows that organic functional groups will be decomposed before 400 °C, and the carbon framework will be completely oxidized at 638.2 °C. Fig. 3(A) shows the weight loss vs temperature of the three samples in air. G/TiO_2 gradually lost 3.3% of weight till 507.3 °C and had a rapid weight loss from 600 to 734 °C. Afterwards the sample weight stabilized at 92.8%. The weight loss before 500 °C was attributed to desorption and/or combustion of hydroxyl groups and organic substances, which were from organic Ti-precursor [44]. The weight ratio of rGO was estimated to be 3.9 wt%. G/ZnO and G/Ta_2O_5 showed similarly thermal stability. Rapid weight loss of 3.7% from rGO combustion in G/ZnO was occurring in the range of 492.7–598.6 °C. For the sample of G/Ta_2O_5, 1.1 wt% of weight loss was observed in the range of 489.0–600.6 °C. Fig. 3(B) confirms the higher stability of rGO in TiO_2 than G/ZnO or G/Ta_2O_5. The exothermic peak from rGO combustion in G/TiO_2 was at 662.9 °C, while that of G/ZnO appeared at 554.6 °C. No significant exothermic peak was found in G/Ta_2O_5 profile, possibly due to lower weight ratio of rGO. The low loading level of rGO on Ta_2O_5 was attributed to the calcination process in the preparation, in which rGO was partially decomposed at 500 °C in 5 min.

Fig. 4 displays FTIR spectra of GO, G/TiO_2, G/ZnO, and G/Ta_2O_5. GO usually has various functional groups, such as aromatic C—H bonds, epoxy, organic carbonate, alcoholic OH, aromatic C=C bonds, C=O, and C—OH, etc. [45]. For the synthesized GO in this investigation, O—H stretching at 3000 cm^{-1}, C—O stretching at 1030 cm^{-1}, and C—OH stretching at 1165 cm^{-1}, were clearly observed. After

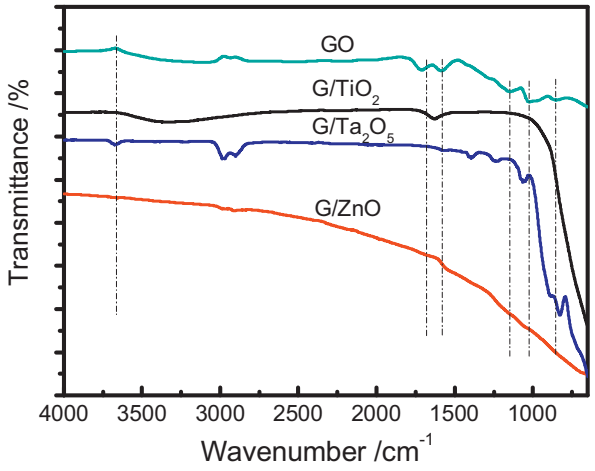

Fig. 4. FTIR spectra of GO and rGO/photocatalyst composites.

formation of composites, most of the above peaks disappeared, indicating the transformation of GO to rGO. In G/Ta_2O_5, the absorption bands at 600–800 cm^{-1} correspond to Ta—O—Ta and Ta—O bands, and 1070 cm^{-1} refers to Ta—O terminal group. The bands in 800–1000 cm^{-1} are from the presence of several suboxides [39]. It was also observed that there were several peaks centered at 1350 and 3000–2800 cm^{-1}, which were attributed to feature distinctive stretching, vibration modes of C—C and the stretching vibration mode of C—H, respectively. The peaks from organic groups might be from CTAB in the preparation of samples.

Fig. 5 shows UV–vis DRS of rGO/photocatalyst composites. It is well known that three pure photocatalysts (TiO_2, ZnO and Ta_2O_5) can only be activated by UV, due to the wide band gap energies of TiO_2 (3.20 eV) [6,38,44], ZnO (3.20 eV)[9], and Ta_2O_5 (4.00 eV) [46,47]. In this study, the band gap energies of TiO_2, ZnO and Ta_2O_5 were estimated to be 3.12, 3.19 and 3.90 eV, respectively. After formation of a composite with rGO, the absorption thresholds of TiO_2, ZnO and Ta_2O_5 were extended to 454.2, 447.0 and 338.1 nm, respectively. The band gap energies were estimated to be 2.73, 2.77 and 3.67 eV, respectively, using the Kubelka–Munk theory [16,38]. DRS results show that, after hybridization with rGO, the absorption edges of TiO_2 and ZnO were shifted to visible light region, while that of Ta_2O_5 remained within UV region.

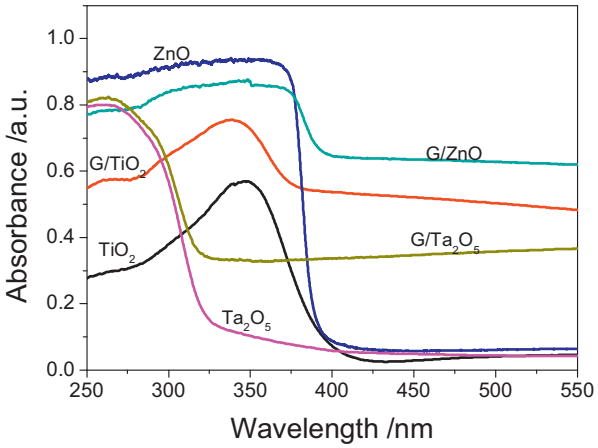

Fig. 5. UV–vis DRS of photocatalysts and their composites.

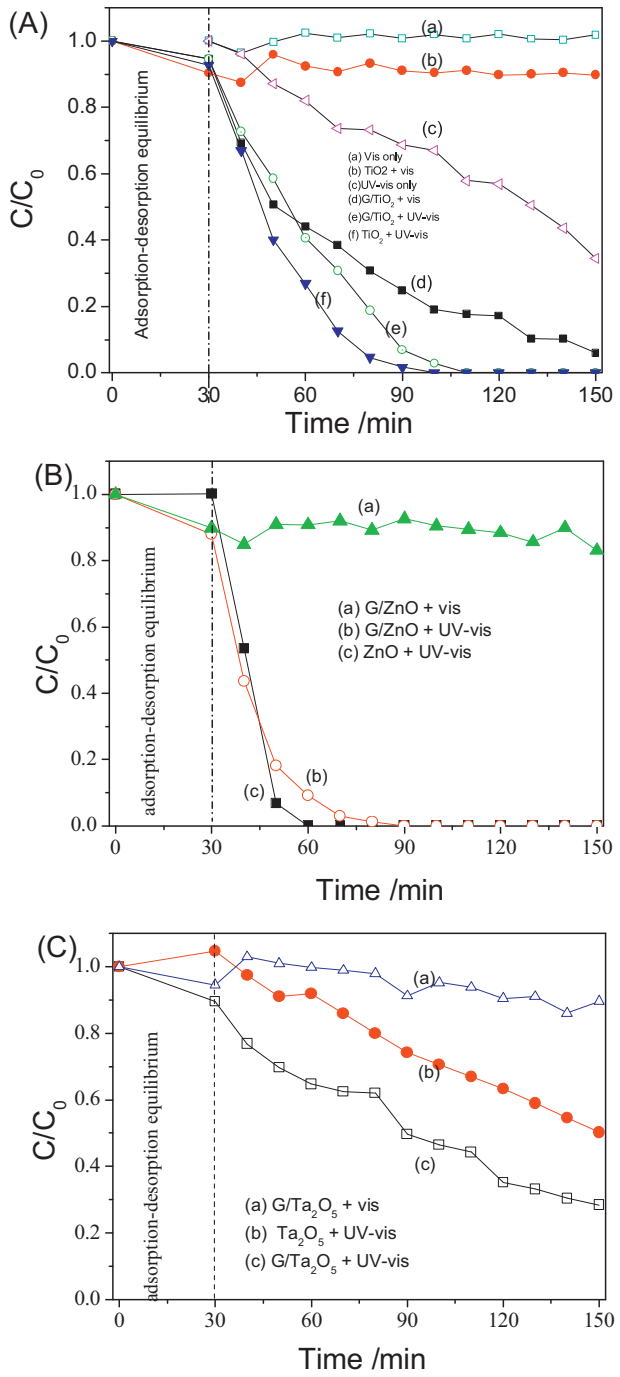

Fig. 6. Photocatalytic oxidation of methylene blue at various conditions. (A) TiO_2 and G/TiO_2: (a) visible light only, (b) TiO_2 and visible light, (c) UV–visible light only, (d) G/TiO_2 and visible light, (e) G/TiO_2 and UV–visible light, and (f) TiO_2 and UV–visible light. (B) ZnO and G/ZnO: (a) G/ZnO and visible light, (b) G/ZnO and UV–visible light, and (c) ZnO and UV–visible light; (C) Ta_2O_5 and G/Ta_2O_5: (a) G/Ta_2O_5 and visible light, (b) Commercial Ta_2O_5 and UV–visible light, and (c) G/Ta_2O_5 and UV–vis light.

3.2. Degradation of methylene blue using rGO/photocatalyst composites

3.2.1. Photocatalytic degradation of methylene blue

Fig. 6 shows the photocatalytic performances of rGO/photocatalyst composites in degradation of MB under UV–vis and visible light irradiations. Fig. 6(A) shows that photolysis by visible light without a catalyst was unable to degrade MB. Unmodified TiO_2 showed about 10% MB removal, which was due to adsorption. UV–vis light could significantly degrade MB, providing 65.1% of MB degradation at 150 min. The hybridization of rGO to TiO_2 made G/TiO_2 effectively decompose MB under visible light. About 94.1% of MB was decomposed by G/TiO_2 after 120 min under visible light. Under UV–vis irradiations, the efficiency of MB degradation was increased both on TiO_2 and G/TiO_2, and 100% MB removal was achieved on both photocatalysts at 110 min. The photocatalytic degradation of MB under visible light was described by first order reaction kinetics and the reaction rate constant of G/TiO_2 + vis was 0.01595 min^{-1} (R^2 = 0.979). Under UV–vis irradiations, the reactions would be zeroth order kinetics. The rate constants for G/TiO_2 + UV–vis and TiO_2 + UV–vis were calculated to be 0.1169 (R^2 = 0.980) and 0.1324 (R^2 = 0.981) ppm/min, respectively. Mohamed et al. [48] reported that the photocatalytic degradation of MB by a modified TiO_2 under UV followed first order rate kinetics. Nolan et al. [49] reported that degradation of MB by N-TiO_2 under visible light also followed first order kinetics. Zeroth order kinetics was observed in photobleaching MB on mesoporous titania films [50].

Fig. 6(B) shows that MB adsorption occurred on G/ZnO and that 11.0% of MB was removed after 30 min, similar to G/TiO_2. Under visible light, however, G/ZnO was not effective in degradation of MB and only 6% of MB was degraded by 120 min photocatalytic reaction. ZnO and G/ZnO showed much higher activity under UV than TiO_2 and G/TiO_2. 100% of MB decomposition was achieved after 30 min on ZnO, and 60 min on G/ZnO. Xu et al. [33] demonstrated that the hybridization with graphene on the surface of commercial ZnO could significantly increase the photocatalytic activity of ZnO under UV lights. Visible-light-driven photocatalytic activity of ZnO/rGO nanocomposite via a microwave-assisted route was also reported [32]. Neither significant enhancement under UV–vis nor visible light photocatalytic activity was observed in this study. High adsorption of G/ZnO in visible light region might be attributed to little amount of metallic zinc, which promotes both light absorption and carriers combination.

Fig. 6(C) shows that G/Ta_2O_5 was not effective to degrade MB under visible light, due to the wide band gap of 3.67 eV. Under UV–vis, Ta_2O_5 could only degrade 50.2% of MB after 120 min. An enhanced efficiency was found on G/Ta_2O_5 for degradation of MB under UV–vis, and 72.1% of MB was decomposed after 120 min. However, the overall activity of Ta_2O_5 or its composite was not as good as ZnO or TiO_2 and their composites. In the preparation, commercial Ta_2O_5 powders were used for G/Ta_2O_5, unlike G/TiO_2 and G/ZnO. It was recalling that the enhancement of photocatalytic activity from rGO was mostly observed in the studies using available photocatalysts (P25 TiO_2, ZnO, SnO_2, etc.) as precursors [28–30,40,51].

The interface structure, optical and morphological properties controlled by the preparation protocol, would be a critic step for the enhanced photocatalytic activity from rGO hybridization [52]. The enhanced photocatalytic activity can be attributed to (i) improved adsorption ability by incorporation of graphene, (ii) extended absorption edge, (iii) unique interface structure for higher charge separation, and (iv) reduced charge combination rate [27,28,30].

3.2.2. Photochemical oxidation of methylene blue

From the above results, G/TiO_2 exhibited photocatalytic activity in visible light while other two only demonstrated activity under UV–vis light. Thus, G/TiO_2 was further investigated for degradation of MB under visible light in photochemical reaction with different oxidants. The effect of oxidants on the efficiency of MB degradation is shown in Fig. 7(A). The oxidants, e.g., PMS, PDS and H_2O_2 behaved differently in the photochemical degradation of MB. 100% of MB removal was achieved with the addition of PDS at 100 min. The reaction time for complete removal of MB was significantly

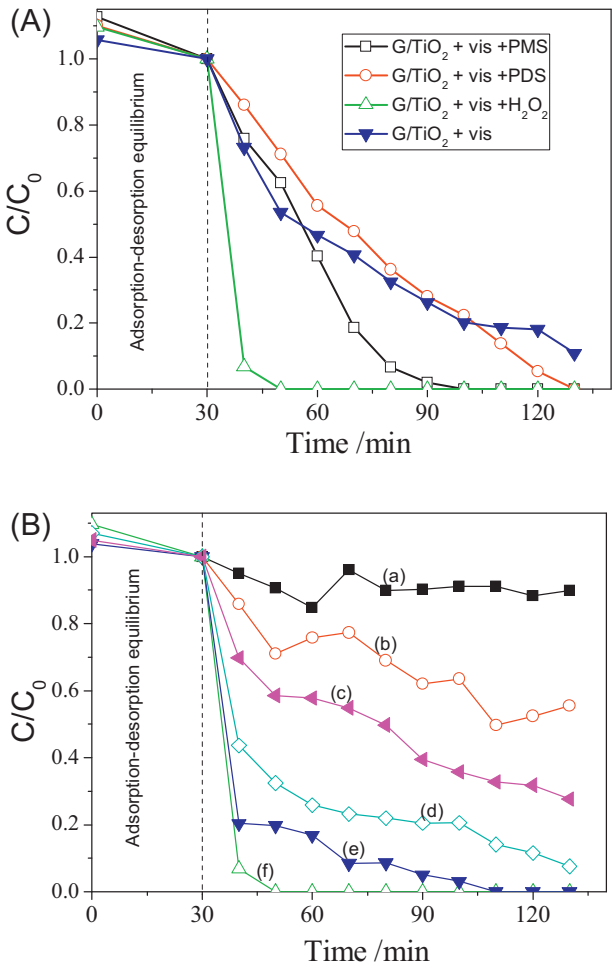

Fig. 7. Photochemical oxidation of methylene blue at various conditions. (A) Effect of oxidants, (B) effect of amount of H_2O_2: (a) 0.338 mol/L H_2O_2 only, (b) 0.338 mol/L H_2O_2 and visible light, (c) G/TiO_2 and vis and 0.050 mol/L H_2O_2, (d) G/TiO_2 and vis and 0.147 mol/L H_2O_2, (e) G/TiO_2 and vis and 0.250 mol/L H_2O_2, and (f) G/TiO_2 and vis and 0.338 mol/L H_2O_2.

reduced to 70 min by the addition of PMS. H_2O_2 showed the best performance for promoting the photocatalytic oxidation of MB with G/TiO_2 under visible light, providing complete MB removal in 20 min. The above results suggest that PDS showed slightly negative effect on MB degradation, while both PMS and H_2O_2 were able to increase MB removal rate under visible light.

We previously reported the varying behavior of H_2O_2, PDS and PMS for promoting degradation of organic pollutants using UV/ZnO [8]. It was found that homogeneous photochemical oxidation of phenol using PMS, PDS or H_2O_2 exhibited much better performance than heterogeneous photocatalytic oxidation using UV/ZnO. The study of combination of photocatalytic/photochemical reactions of UV/ZnO/oxidant suggested that PDS and H_2O_2 imposed a negative effect on UV/ZnO, while PMS was able to increase the efficiency of phenol degradation. Under UV irradiation, H_2O_2 will be activated to produce hydroxyl radicals [1].

$$H_2O_2 + h\nu \rightarrow 2\,{}^{\cdot}OH \quad (1)$$

PDS and PMS can produce sulfate radicals by UV activation as follows [8].

$$S_2O_8^{2-} + h\nu \rightarrow 2SO_4^{\cdot -} \quad (2)$$

$$HSO_5^{-} + h\nu \rightarrow SO_4^{\cdot -} + {}^{\cdot}OH \quad (3)$$

In photocatalytic reactions, either TiO_2 or ZnO, would produce oxidative radicals under radiations. Therefore, the competitive reaction of free radicals between pollutant molecules and other chemical species would determine the effect of the oxidant. For example, in the system of UV/ZnO/PMS or UV/ZnO/H_2O_2 [8,53], the following reactions also occur.

$$HSO_5^{-} + {}^{\cdot}OH \rightarrow SO_5^{\cdot -} + H_2O \quad (4)$$

$$H_2O_2 + {}^{\cdot}OH \rightarrow H_2O^{\cdot} + H_2O \quad (5)$$

The produced $SO_5^{\cdot -}$ and $H_2O^{\bullet}$ have less oxidative potential than $SO_4^{\cdot -}$ and ·OH, resulting in a lower efficiency in oxidation of organics.

It was also found that the light source would influence the effect of oxidant on the efficiency of pollutant degradation. For example, PDS could provide a positive enhancement to ZnO for oxidation of phenol under artificial sunlight [54]. A recent study further discovered that even for the same oxidant and reaction condition, the oxidant behaved differently onto varying photocatalysts [10].

In this study, visible light was used and it was not surprised to find the negative effect of PDS, positive effect of PMS and significant enhancement of H_2O_2 to the system of G/TiO_2 + vis. Moreover, PDS and PMS can be activated by visible light for oxidation [10], indicating sulfate radicals are produced. However, visible light could hardly activate H_2O_2 [55]. Therefore, the quenching reactions between radicals would be minimized on H_2O_2. The enhancement of H_2O_2 was possibly due to the activation by electrons from G/TiO_2 [56].

$$TiO_2 + rGO* + vis \rightarrow e_{cb}^{-}(TiO_2) + rGO*^{+} \quad (6)$$

$$H_2O_2 + e_{cb}^{-} \rightarrow {}^{\cdot}OH + {}^{-}OH \quad (7)$$

Therefore, enhancement of H_2O_2 was ascribed to the produced hydroxyl radicals from effective trapping of photoinduced carriers.

Fig. 7(B) further shows the effect of H_2O_2 amount on the degradation rate of MB. Without a catalyst and light, H_2O_2 exhibited little MB degradation. Under visible light, H_2O_2 itself showed a moderate decomposition of MB. Li et al. [56] experimentally demonstrated that H_2O_2 could not be decomposed under visible light irradiation without TiO_2 or in the dark in the presence of TiO_2. Similar results were obtained in the visible-light-degradation of malachite green [55]. In this study, the electrons for the excited states of MB under visible light might be transferred to H_2O_2, leading to the formation of hydroxyl radicals for oxidation. The degradation rate increased with increasing H_2O_2 amount, implying that reaction of Eq. (5) hardly occurred and that all H_2O_2 contributed to trapping electrons for producing hydroxyl radicals.

4. Conclusions

Various composites of G/TiO_2, G/ZnO, and G/Ta_2O_5, were successfully prepared and their properties were characterized. The absorption edges of TiO_2 and ZnO were extended to visible light region by rGO, however, only G/TiO_2 showed visible light photocatalytic activity. The effect of oxidants on MB degradation under visible light irradiations was investigated. PDS showed a weakly negative effect, while PMS and H_2O_2 were able to increase MB degradation rate. The enhancement of H_2O_2 to the system of G/TiO_2 + vis was ascribed to the minimized quenching reactions and the promoted ability in trapping photoinduced carriers.

References

[1] M.I. Stefan, A.R. Hoy, J.R. Bolton, Environmental Science and Technology 30 (1996) 2382–2390.
[2] Y. Lee, U. von Gunten, Water Research 44 (2010) 555–566.
[3] D. Dvoranova, V. Brezova, M. Mazur, M.A. Malati, Applied Catalysis B – Environmental 37 (2002) 91–105.

[4] Q.J. Yang, H. Choi, Y.J. Chen, D.D. Dionysiou, Applied Catalysis B – Environmental 77 (2008) 300–307.
[5] G.P. Anipsitakis, D.D. Dionysiou, Applied Catalysis B – Environmental 54 (2004) 155–163.
[6] H.Q. Sun, Y. Bai, H.J. Liu, W.Q. Jin, N.P. Xu, G.J. Chen, B.Q. Xu, Journal of Physical Chemistry C 112 (2008) 13304–13309.
[7] H.Q. Sun, R. Ullah, S.H. Chong, H.M. Ang, M.O. Tade, S.B. Wang, Applied Catalysis B – Environmental 108 (2011) 127–133.
[8] P. Shukla, I. Fatimah, S.B. Wang, H.M. Ang, M.O. Tade, Catalysis Today 157 (2010) 410–414.
[9] H.Q. Sun, X.H. Feng, S.B. Wang, H.M. Ang, M.O. Tade, Chemical Engineering Journal 170 (2011) 270–277.
[10] G.L. Zhou, H.Q. Sun, S.B. Wang, H.M. Ang, M.O. Tade, Separation and Purification Technology 80 (2011) 626–634.
[11] J. Fernandez, P. Maruthamuthu, J. Kiwi, Journal of Photochemistry and Photobiology A – Chemistry 161 (2004) 185–192.
[12] J. Fernandez, P. Maruthamuthu, A. Renken, J. Kiwi, Applied Catalysis B – Environmental 49 (2004) 207–215.
[13] P.R. Shukla, S.B. Wang, H.Q. Sun, H.M. Ang, M. Tade, Applied Catalysis B – Environmental 100 (2010) 529–534.
[14] P. Shukla, H.Q. Sun, S.B. Wang, H.M. Ang, M.O. Tade, Catalysis Today 175 (2011) 380–385.
[15] H.Q. Sun, H.Y. Tian, Y. Hardjono, C.E. Buckley, S.B. Wang, Catalysis Today 186 (2012) 63–68.
[16] H.Q. Sun, S.B. Wang, H.M. Ang, M.O. Tade, Q. Li, Chemical Engineering Journal 162 (2010) 437–447.
[17] L.W. Zhang, H.B. Fu, Y.F. Zhu, Advanced Functional Materials 18 (2008) 2180–2189.
[18] S. Sakthivel, B. Neppolian, M.V. Shankar, B. Arabindoo, M. Palanichamy, V. Murugesan, Solar Energy Materials and Solar Cells 77 (2003) 65–82.
[19] Z.F. Zhu, F. Yu, Y. Man, Q.Y. Tian, Y. He, N.Z. Wu, Journal of Solid State Chemistry 178 (2005) 224–229.
[20] D. Li, H. Haneda, Journal of Photochemistry and Photobiology A – Chemistry 155 (2003) 171–178.
[21] G.C.C. Yang, S.W. Chan, Journal of Nanoparticle Research 11 (2009) 221–230.
[22] Y.F. Huang, Y.L. Wei, J.H. Wu, C.S. Guo, M. Wang, S. Yin, T. Sato, Applied Catalysis B – Environmental 123 (2012) 9–17.
[23] T. Murase, H. Irie, K. Hashimoto, Journal of Physical Chemistry B 108 (2004) 15803–15807.
[24] Z.H. Li, J.W. Liu, J.Y. Li, J. Shen, Nanoscale 4 (2012) 3867–3870.
[25] L.L. Xu, W.D. Shi, J.G. Guan, Catalysis Communications 25 (2012) 54–58.
[26] M.J. Allen, V.C. Tung, R.B. Kaner, Chemical Reviews 110 (2010) 132–145.
[27] W.G. Wang, J.G. Yu, Q.J. Xiang, B. Cheng, Applied Catalysis B – Environmental 119 (2012) 109–116.
[28] H. Zhang, X.J. Lv, Y.M. Li, Y. Wang, J.H. Li, ACS Nano 4 (2010) 380–386.
[29] V. Stengl, D. Popelkova, P. Vlacil, Journal of Physical Chemistry C 115 (2011) 25209–25218.
[30] J.S. Lee, K.H. You, C.B. Park, Advanced Materials 24 (2012) 1084–1088.
[31] D.L. Zhao, G.D. Sheng, C.L. Chen, X.K. Wang, Applied Catalysis B – Environmental 111 (2012) 303–308.
[32] Y. Liu, Y. Hu, M.J. Zhou, H.S. Qian, X. Hu, Applied Catalysis B – Environmental 125 (2012) 425–431.
[33] T.G. Xu, L.W. Zhang, H.Y. Cheng, Y.F. Zhu, Applied Catalysis B – Environmental 101 (2011) 382–387.
[34] J.F. Wang, T. Tsuzuki, B. Tang, X.L. Hou, L. Sun, X.G. Wang, ACS Applied Materials & Interfaces 4 (2012) 3084–3090.
[35] H. Sun, S. Liu, G. Zhou, H.M. Ang, M.O. Tadé, S. Wang, ACS Applied Materials & Interfaces 4 (2012) 5466–5471.
[36] W.S. Hummers Jr., Hummers, Journal of American Chemical Society 80 (1958) 1339.
[37] J.Y. Jang, M.S. Kim, H.M. Jeong, C.M. Shin, Composites Science and Technology 69 (2009) 186–191.
[38] H.Q. Sun, Y. Bai, W.Q. Jin, N.P. Xu, Solar Energy Materials and Solar Cells 92 (2008) 76–83.
[39] T.C. An, J.K. Liu, G.Y. Li, S.Q. Zhang, H.J. Zhao, X.Y. Zeng, G.Y. Sheng, J.M. Fu, Applied Catalysis A: General 350 (2008) 237–243.
[40] J.K. Liu, T.C. An, G.Y. Li, N.Z. Bao, G.Y. Sheng, J.M. Fu, Microporous and Mesoporous Materials 124 (2009) 197–203.
[41] S. Wakeland, R. Martinez, J.K. Grey, C.C. Luhrs, Carbon 48 (2010) 3463–3470.
[42] R.Y. Hong, T.T. Pan, J.Z. Qian, H.Z. Li, Chemical Engineering Journal 119 (2006) 71–81.
[43] H.C. Huang, T.E. Hsieh, Journal of Applied Polymer Science 117 (2010) 1252–1259.
[44] H.Q. Sun, Y. Bai, Y.P. Cheng, W.Q. Jin, N.P. Xu, Industrial & Engineering Chemistry Research 45 (2006) 4971–4976.
[45] X.B. Fan, W.C. Peng, Y. Li, X.Y. Li, S.L. Wang, G.L. Zhang, F.B. Zhang, Advanced Materials 20 (2008) 4490–4493.
[46] T. Sreethawong, S. Ngamsinlapasathian, Y. Suzuki, S. Yoshikawa, Journal of Molecular Catalysis A: Chemical 235 (2005) 1–11.
[47] M. Stodolny, M. Laniecki, Catalysis Today 142 (2009) 314–319.
[48] M.M. Mohamed, M.M. Al-Esaimi, Journal of Molecular Catalysis A: Chemical 255 (2006) 53–61.
[49] N.T. Nolan, D.W. Synnott, M.K. Seery, S.J. Hinder, A. Van Wassenhoven, S.C. Pillai, Journal of Hazardous Materials 211 (2012) 88–94.
[50] A. Mills, M. Sheik, C. O'Rourke, M. McFarlane, Applied Catalysis B – Environmental 89 (2009) 189–195.
[51] P. Shukla, H.Q. Sun, S.B. Wang, H.M. Ang, M.O. Tade, Separation and Purification Technology 77 (2011) 230–236.
[52] J.Y. Chen, G.Y. Li, Y. Huang, H.M. Zhang, H.J. Zhao, T.C. An, Applied Catalysis B – Environmental 123 (2012) 69–77.
[53] P. Shukla, S.B. Wang, H.Q. Sun, H.M. Ang, M. Tade, Chemical Engineering Journal 164 (2010) 255–260.
[54] P.R. Shukla, S.B. Wang, H.M. Ang, M.O. Tade, Separation and Purification Technology 70 (2010) 338–344.
[55] M.M. Cheng, W.H. Ma, J. Li, Y.P. Huang, J.C. Zhao, Environmental Science and Technology 38 (2004) 1569–1575.
[56] X.Z. Li, C.C. Chen, J.C. Zhao, Langmuir 17 (2001) 4118–4122.